Available online at www.sciencedirect.com
SCIENCE DIRECT
Journal of Power Sources 155 (2006) 420–427
JOURNAL OF POWER SOURCES
www.elsevier.com/locate/jpowsour

Effect of Sn concentration on the corrosion resistance of Pb-Sn alloys in H_2SO_4 solution

Jing Xu [a,b], Xingbo Liu [b,*], Xiaogang Li [a,c], Ever Barbero [b], Chaofang Dong [a]

[a] *Center of Corrosion and Protection, University of Science and Technology Beijing 100083, China*
[b] *Mechanical and Aerospace Engineering Department, West Virginia University, Morgantown, WV 26506, USA*
[c] *State Key Laboratory for Corrosion and Protection, Shenyang 110016, China*

Received 28 February 2005; accepted 2 April 2005
Available online 22 June 2005

Abstract

The effect of Sn concentration on the corrosion resistance of Pb-Sn alloy in H_2SO_4 electrolyte was investigated by potentiodynamic polarization. A new approach to calculate the exchange current density, i_{corr}, was proposed and proved to be in accordance with the experimental results. This study shows that with the increase of alloying Sn, the corrosion rate of the alloy increased and then decreased, with its minimum appearing at 2.60 wt.% Sn. It was also found that the cathodic reaction does not have to be a single-step process, i.e., there are multiple sub-steps involved and complex cations, including H_4^{3+} and H_2^{+}, existing in the systems.
© 2005 Elsevier B.V. All rights reserved.

Keywords: Pb-Sn alloy; Potentiodynaic polarization; Corrosion rate

1. Introduction

Pb-Sb alloy has long been used as grid materials in lead acid batteries because of its good casting and deep cycling properties [1]. However, Sb introduces a poisonous effect on electrodes, which is fatal to the batteries' rechargeable life. Various alternative alloys, including Pb-Ca, Pb-Ca-Al, and Pb-Ag, have been proposed to replace Pb-Sb alloys as grid materials during the last two decades [2–5]. Among them, Pb-Ca alloy is the most popular one for its high overpotential to hydrogen evolution reaction and low cost. Pb-Ca alloy has been proven to restrain a battery's self-discharge and decrease the amount of cathodic evoluted hydrogen during the charge process, resulting in an excellent maintenance-free property. In addition, the conductivity and low-temperature applicability of Pb-Ca alloys are better than that of Pb-Sb alloys [6].

Typical Pb-Ca alloys have very fine grains, which leads to excessive grain boundary areas and fast intergranular corrosion [7], therefore, Ca contents have to be carefully controlled to avoid excessive amounts which would provide an alloy composition that has an unduly high tendency to recrystallize after solidification [8]. Sn has been proved to improve the corrosion resistance of Pb-Ca alloys [4–6,9–11], and improve the charge-discovering ability after overdischarge and standing [8]. It has been reported that the anti-corrosive property of Pb-Ca-Sn mainly depends on the ratio of Sn/Ca [9,10]. Alloys with a low Sn/Ca ratio (less than 9) have high corrosion rates and fine grains, while a high Sn/Ca ratio (more than 9) have low corrosion rates and coarse grains. The same conclusion has been drawn in Pb-Ca-Sn-Ag alloys [12]. It has been shown that alloying Sn can slow down the corrosion rate and promote growth of the compact passive layer [13].

Since the composition and morphology of corrosion layer of the grid materials strongly affect the performance and service life of lead acid batteries, the details of this layer for Pb and Pb-Sb alloys have been extensively studied during the last decade [14,15]. It was found that the corrosion layer of Pb is different in various concentrations of the H_2SO_4

* Corresponding author. Tel.: +1 304 2933111x2324; fax: +1 304 2936689.
E-mail address: xingbo.liu@mail.wvu.edu (X. Liu).

0378-7753/$ – see front matter © 2005 Elsevier B.V. All rights reserved.
doi:10.1016/j.jpowsour.2005.04.026

solution [15]. Three acid concentration regions can be distinguished: (a) active acid concentration region ($5.0\,M > C_{H_2SO_4} > 0.5\,M$), where drop-like β-$PbO_2$ is formed; (b) passive high concentration region ($C_{H_2SO_4} > 5.0\,M$), where crystal-shaped α-PbO_2 is formed; and (c) passive low concentration region ($C_{H_2SO_4} \leq 0.5\,M$), where PbO_2 particles are crystal-shaped and are interconnected in dendrites. In terms of Pb-Sb alloys, the corrosion layers of these alloys include $PbSO_4$ and lead oxides: PbO, PbO_n, PbO_2, as well as $Pb_{1-x}SbO_xO_n$, $Pb_{1-x}Sb_xO_2$ [16]. It was established that Sb has a catalytic effect on the reaction $PbO \rightarrow PbO_n$ ans slows down the rate of the reaction $PbO_n \rightarrow PbO_2$.

The investigations on Sn in Pb-based alloys have shown the potential to use Pb-Sn alloys as a grid material in Pb acid batteries. The purpose of this investigation is to study the effect of Sn concentrations on the corrosion resistance and pitting sensitivity of a Pb-Sn alloy in H_2SO_4 aqueous electrolyte, which is very essential to the application of Pb-Sn alloy grids in lead acid batteries.

2. Experiments

2.1. Materials

Pure casting Pb (99.99 wt.%) and five Pb-Sn alloys with different tin component levels were used as the working electrodes. Pb-Sn alloys were cast by using high purity Pb (99.99 wt.%) and Sn (99.9 wt.%). The compositions of the specimens are listed in Table 1.

2.2. Potentiodynamic polarization tests

A test sample was cut in the shape of cubic ($1\,cm \times 1\,cm \times 1\,cm$) from each alloy. An electrical connection was provided by soldering a Cu wire to one end of the specimen. The soldered joint and sides of the specimen were later sealed off with Araldite adhesive to expose a square area of $1\,cm^2$. The surface of the working electrodes was mechanically polished with sand paper, and then rinsed with distilled water and placed into the cell for potentiostatic and potentiodynamic polarization tests. Fig. 1 shows the sketch of the test setup. The electrolyte was a 4.0 mol/l H_2SO_4 solution prepared from AR grade sulfuric acid and distilled water. A Pt plate served as the counter electrode. The reference electrode

Table 1
Chemical composition of six Pb-Sn alloys (wt.%)

Sample no.	Sn wt.%
0	0
1	0.532
2	0.820
3	1.06
4	1.57
5	2.60
6	4.68

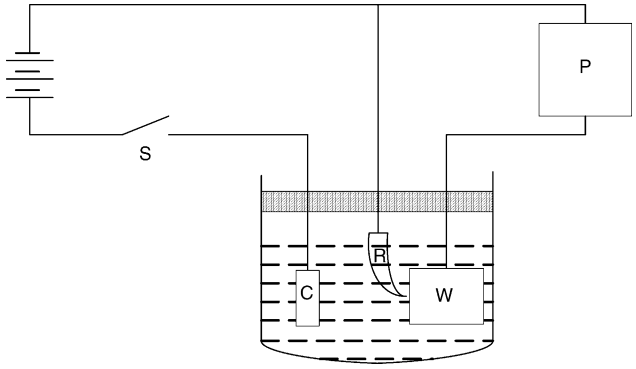

Fig. 1. Sketch of the electrochemical testing setup (C, counter electrode; R, reference electrode; W, working electrode).

was the Hg/Hg_2Cl_2 electrode (SCE). All potentials reported here are referred to the Hg/Hg_2Cl_2 reference electrode.

A cathodic polarization at −1.2 V for 20 min was performed to remove any oxidation products formed during the pretreatment. The potentiostatic polarization was performed at the fixed potential of 0.60 V for 1 h. The potentiodynamic polarization, with scanning speed of 1 mV/s, began with a potential of −1.5 V, and ended with a potential of +2.3 V. Electrochemical potentiostatic and potentiodynamic polarization curves were measured and recorded using EG&G PARC 273 potentiostat/galvanostat controlled by EG&G PARC 273 software. All experiments were performed at $25 \pm 2\,^{\circ}C$.

3. Experimental results

3.1. Microstructure of Pb-Sn alloys

Pure casting Pb appears as a relatively loose microstructure, with a very small amount of inclusions. According to the Pb-Sn phase diagram, shown in Fig. 2 [17], the microstructure of all tested Pb-Sn alloy specimens was $\alpha + \beta$. The density of

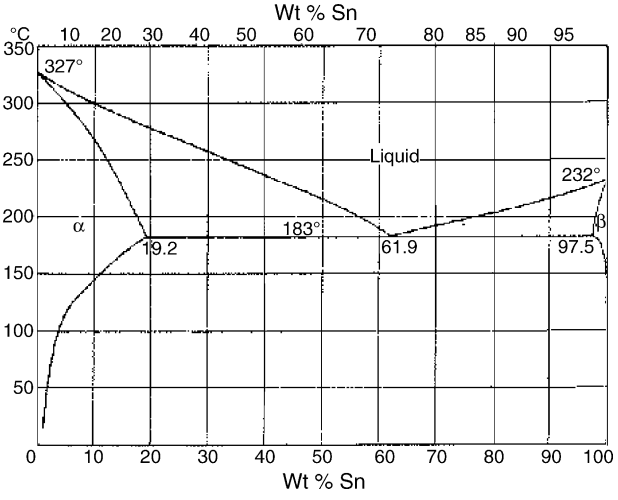

Fig. 2. Pb-Sn phase diagram [17].

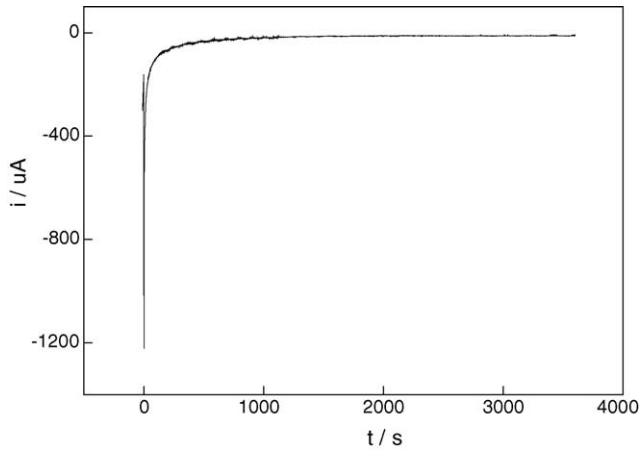

Fig. 3. Potentiostatic polarization curve of Pb-Sn alloys in 4 M H_2SO_4 solution (Pb-0.532 wt.% Sn, $E = 0.6$ V, $t = 1$ h).

β increases as the concentration of Sn increases. Small strips of β are formed when the Sn contents are higher than 1 wt.%.

3.2. The polarization curves of Pb-Sn alloys in 4 M H_2SO_4 solution

From Pb-Sn alloys' potentiostatic and potentiodynamic polarization curves, as plotted in Fig. 3 (taking No. 1 Pb-0.532 wt.% Sn as the example) and Fig. 4, the oxidation part shows the characteristic of the passivation property of Pb-Sn alloys. Passive currents of these seven different samples are shown in Table 2. Based on the experimental data, potentiostatic charge of the corrosion layer to these alloys is calculated and the details of these calculations are presented in Section 4.1.

Table 2
Passive currents in potentiostatic curves of Pb-Sn alloys in 4 M H_2SO_4 solution

Sn wt.%	Passive current (uA)
0	10
0.532	12
0.820	38
1.06	22
1.57	15
2.60	14
4.68	27

After the passivation process the continuous passive layer is destroyed and pitting occurs. Corresponding electrochemical parameters, equilibrium potential (E^0), pitting potential (E_p), and the difference between E^0 and E_p ($E_p - E^0$), which are derived from the experimental data, are collected in Table 3. According to the test results, the value of E_p is around 1.65 V while interzone spanning from E_p to E^0 is more than 2 V. This data indicates that all tested Pb-Sn alloys have good anti-corrosive properties, although pitting does occur after compact passive layers are penetrated. Once pitting starts, the sulfuric acid, which acts as an electrolyte, infiltrates the protective layers and promotes the electrochemical reaction acting as so-called self-catalysis [18].

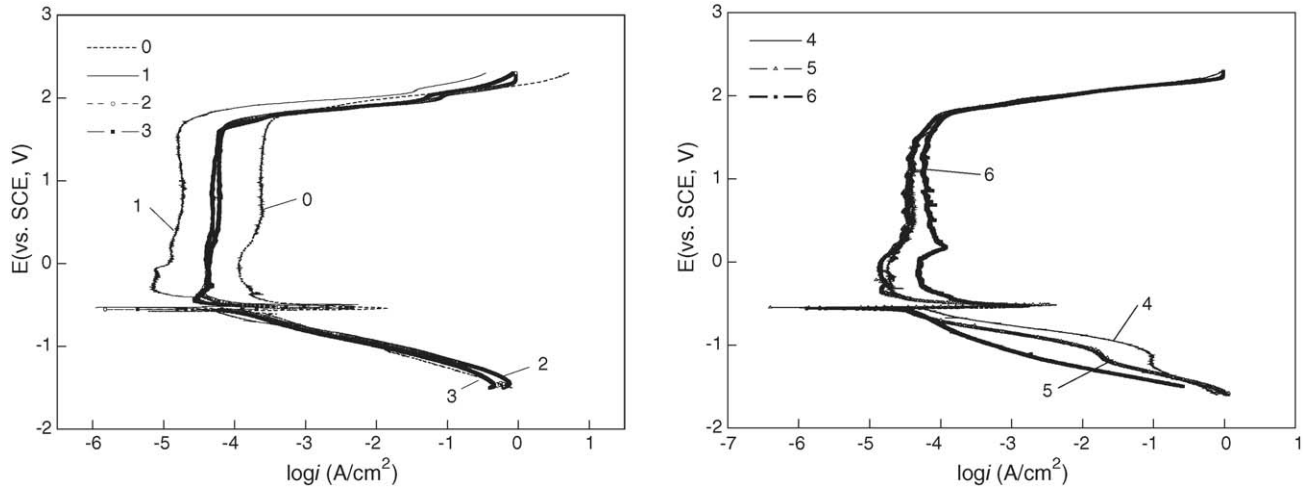

Fig. 4. Potentiodynamic polarization curves of Pb-Sn alloys in 4 M H_2SO_4 solution. (0), Pure Pb; (1), Pb-0.532 wt.% Sn; (2), Pb-0.82 wt.% Sn; (3), Pb-1.06 wt.% Sn; (4), Pb-1.57 wt.% Sn; (5), Pb-2.60 wt.% Sn; (6), Pb-4.68 wt.% Sn.

Table 3
Characteristic parameters of polarization curves of Pb-Sn alloys in 4 M H_2SO_4 solution

	Sample no.						
	0	1	2	3	4	5	6
Equilibrium potential E^0 (V vs. SCE)	−0.577	−0.531	−0.554	−0.556	−0.543	−0.550	−0.563
Pitting potential E_p (V vs. SCE)	1.722	1.692	1.622	1.621	1.657	1.675	1.651
Difference between E_p and E^0 (V)	2.299	2.223	2.162	2.193	2.200	2.225	2.214

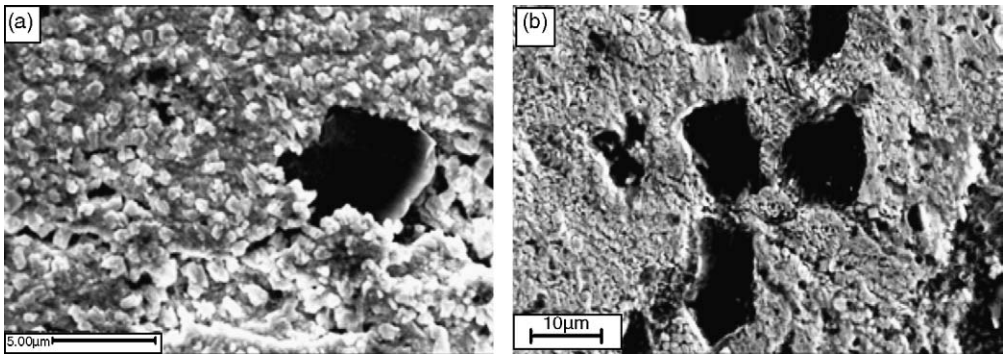

Fig. 5. Micrographs of pittings in pure Pb and Pb-Sn alloy. (a) 99.99 wt.% Pb and (b) Pb-2.60 wt.% Sn.

3.3. Pitting of Pb-Sn alloys in 4 M H_2SO_4 solution

Fig. 5 shows the SEM micrographs of the passive layers of pure Pb and Pb-2.60 wt.% Sn. The passive layer of pure Pb is denser, with sporadical pittings on its surface (Fig. 5a), when compared with Pb-Sn alloys on which dispersed pitting holes of different sizes (Fig. 5b) can be observed. It was proposed that the reason why Pb-Sn alloys have severe pitting is mainly due to the intergranular corrosion caused by the alloying tin, which prevents passivation from keeping consistent [19,20]. Sn(II) and Sn(IV) subside along the grain boundaries of passive products, such as $PbSO_4$ and $PbO{\cdot}PbSO_4$ [21,22], while some Sn(II) is precipitated in the PbO lattice [23,24]. This inserted Sn increases the pitting sensitivity of the passive layer, leading to worse anti-corrosive abilities, but better conductivity.

4. Discussions

4.1. Calculation of passive layer's thickness

Passive layer growth of the tested alloys was estimated by simplifying the oxidation reaction as: $xM - xye^- \rightarrow xM^{y+}$, with $d\delta/dt = iM_{ox}/y\rho F$, where M_{ox} is molar mass of the oxidized product; i is the passive current density, and δ and ρ are the passive layer's thickness and density respectively. When the composition of the passive layer and passive current density are known, the passivation rate $d\delta/dt$ is fixed. The investigation of the passive layer by XPS shows that its composition is complex and the ratio of different ingredients vary [29]. Assuming that the corrosion layer was mostly chemically corroded and consisted of predominately $PbSO_4{\cdot}PbO_2$, and PbO, respectively, the thickness of the passive layers were calculated and are summarized in Table 4. Taking an example of PbO as 100% passive layer, the relationship between Sn contents and passive layer's thickness is perceived in Fig. 6.

Table 4
Passive layer's thickness from potentiostatic curves of Pb-Sn alloys in 4 M H_2SO_4

	ID						
	0	1	2	3	4	5	6
Sn wt.%	0	0.532	0.820	1.06	1.57	2.60	4.68
$PbSO_4$ thickness (nm)	4.98	5.97	18.90	10.94	7.45	6.97	13.44
PbO_2 thickness (nm)	1.96	2.36	7.46	4.32	2.94	2.75	5.30
PbO thickness (nm)	3.66	4.39	13.91	8.05	5.49	5.15	9.88

4.2. Calculation on exchange current density i_{corr}

Based on basic electrochemical concepts, the redox couple takes effect in the corrosion system. If both of the equilibrium potentials for the redox reaction are far from E^0, the Tafel zone appears to be standard linear when the scanning potential in the potentiodynamic polarization process is close to a zero-charge potential (E^0). Under this condition, the electrochemical process is the mixed result controlled by both the anodic reaction and the cathodic reaction.

Normally, it is difficult to calculate the exchange current density (i_{corr}) directly due to the difficulty of finding the ideal anodic Tafel zone. In this paper, a new approach is proposed to calculate i_{corr} by using a tested cathodic Tafel line and a weak polarization area. Other electrochemical parameters,

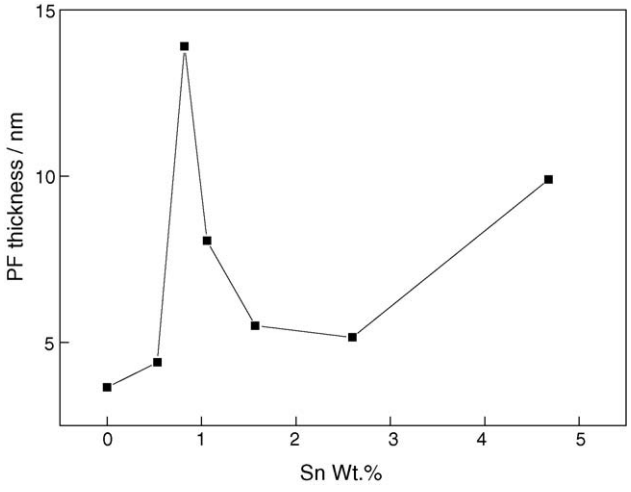

Fig. 6. Relationship between Sn contents and passive layer's thickness.

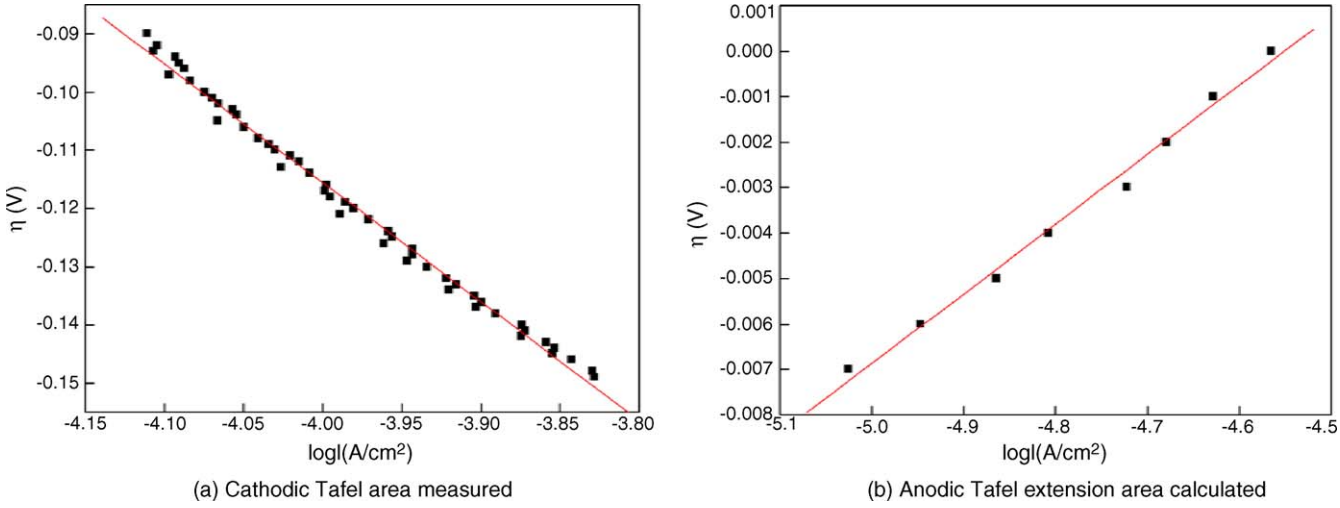

Fig. 7. Relationship between overpotential (η) and the current density (*i*) in Tafel area of No. 1 specimen containing 0.532 wt.% Sn.

such as n, a_A, and b_A, can also be calculated as by-products of this method. Details about the calculation are outlined below.

The electrochemical corrosion of Pb-Sn in H_2SO_4 involves oxidation of the alloys in the anode and reduction of hydrogen cations in the cathode. The formulas of the anodic and cathodic reactions are written as:

$$\text{Anode}: \quad M = M^{x+} + xe \tag{a}$$

$$\text{Cathode}: \quad 2H^+ + 2e = H_2 \tag{b}$$

In the standard polarization zone (Tafel zone), the relationship between the polarization current (i) and the overpotential (η) exist as:

$$\eta_C = a_C + b_C \times lg\, i_C \tag{1}$$

$$\eta_A = a_A + b_A \times lg\, i_A \tag{2}$$

where the subscripts C and A correspond to the cathode and anode, respectively; a is the intercept of the linear Tafel plot, while b, is the slope.

The parameters a_C, b_C, a_A, and b_A are defined as:

$$a_C = \frac{2.3RT}{\alpha_1 nF} lg\, i_{Corr}, \quad b_C = \frac{2.3RT}{\alpha_1 nF} \tag{3}$$

$$a_A = -\frac{2.3RT}{\beta_2 nF} lg\, i_{Corr}, \quad b_A = \frac{2.3RT}{\beta_2 nF} \tag{4}$$

where α_1, β_2 represent the transport coefficient of the reduction and oxidation, with the relationship $\alpha + \beta = 1$. Normally, both α_1 and β_2 are roughly settled as 0.5 during the calculation. From Eqs. (3) and (4) above, i_{corr} is given by:

$$\log i_{Corr} = -\frac{a_C}{b_C} = \frac{a_A}{b_A} \tag{5}$$

Therefore, once the intercept, a, and the slope, b, of either the cathodic Tafel line or anodic are obtained, its i_{corr} can be derived. Here, anodic parameters a_A and b_A are set by using the cathode weak polarization zone which is outlined below.

Table 5
Calculation results of parameters shown in Fig. 6(a)

	Parameter				
	A	*B*	*R*	S.D.	*N*
Value	−0.93375	−0.20453	−0.99655	0.00145	52
Error	0.00959	0.00241			

Note: $E = A + B$; R is the confidence; S.D. is the standard deviation; N is the number of data.

Cathodic polarization current (i_C), which is revealed in the potentiodynamic experiment, is the result of both the reduction current (i_2) and oxidation current (i_1) as, $i_C = i_2 - i_1$. By extending the cathodic Tafel line to its weak polarization zone, we can calculate i_2 in this narrow area. Applying the tested i_C with the equation $i_1 = i_2 - i_C$, i_1 is derived under its corresponding overpotential. Thus, i_1 is also regarded as the result extended from the anodic Tafel area to the cathodic one. Accordingly the anodic Tafel line is calculated, along with its intercept, a_A, and slope, b_A. Now using the calculated values of a_A and b_A, i_{corr} can be double checked to ensure its accuracy, based on Eq. (4). If the two values of i_{corr}, calculated by Eqs. (3) and (4), are close, the cathodic Tafel area selection is correct. Otherwise, re-select the cathodic Tafel line part from the tested polarization curve and repeat the calculation above until the results are satisfactory. In addition, Eqs. (3) and (4) also give a clue in calculating the amount of the transferred electrons (n) in the dominating step of the redox couple.

Taking sample No. 1 as an example, the calculation and related results are shown in Fig. 7, and Tables 5 and 6. The

Table 6
Calculation results of parameters shown in Fig. 6(b)

	Parameter				
	A	*B*	*R*	S.D.	*N*
Value	0.0696	0.01529	0.99591	2.39061E-4	8
Error	0.00271	5.66424E-4			

Table 7
Calculation results of all six Pb-Sn alloys

Sample no.	i_{corr-C} (mA/cm^2)	i_{corr-A} (mA/cm^2)	i_{corr} (mA/cm^2)	b_C (V)	b_A (V)	n_C
1	2.72054E−5	2.80547E−5	2.763E−5	−0.20453	0.01529	−0.56767
2	7.79037E−5	8.09082E−5	7.9406E−5	−0.20647	0.01076	−0.56234
3	6.50531E−5	7.09858E−5	6.80194E−5	−0.21571	0.01579	−0.53825
4	1.49735E−5	1.85478E−5	1.67607E−5	−0.12263	0.00205	−0.9468
5	1.8278E−5	1.36482E−5	1.59631E−5	−0.22884	0.00459	−0.50737
6	3.76553E−5	3.75224E−5	3.75888E−5	−0.46066	0.04193	−0.25204

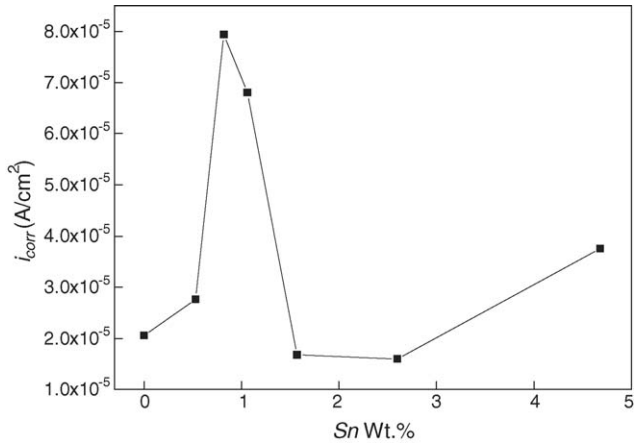

Fig. 8. Relationship between Sn contents and i_{corr}.

same calculation method was applied to all of the alloys. The data is summarized in Table 7.

4.3. Effect of Sn Concentration on the passivation and corrosion of Pb-Sn alloys

Fig. 8 shows the effect of the Sn content on i_{corr}, which is propotional to the alloys' self-corrosion rate. The relationship between the weight percent of Sn and the pitting potential (E_p) is shown in Fig. 9. In terms of i_{corr}, the order from the maximum to minimum is as follows: Nos. 2, 3, 1, 6, 4 and 5. From Fig. 6, we conclude that i_{corr} of Pb-Sn alloys increase and

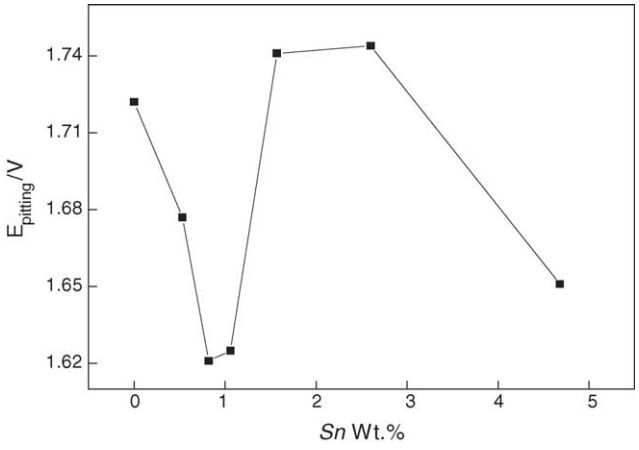

Fig. 9. Relationship between Sn contents and E_p.

then decrease as alloying tin's concentration goes up. When the weight percent of Sn is around 0.8 wt.%, i_{corr} reached its maximum. It should be pointed out that the comparison between Fig. 9 (Sn content versus i_{corr}) and Fig. 6 (Sn content versus passive layer thickness) shows that they have the same trend, which provides the indirect proof of the calculation on i_{corr} discussed above.

The effect of Sn on the anti-corrosion properties of Pb-Sn alloy can be discussed in two-fold [24,25]: conductivity and ion transportation. Transportation of ions and electrons in the passive layer are the two most important processes to determine the corrosion rate of the alloys and the slower process between these two could be the controlling step of the corrosion reaction. It has been found that Sn can improve the conductivity of Pb-Sn alloys' passive film by promoting the formation of PbO_x ($1 < x < 2$) [26], which has a resistance lower than both $PbSO_4$ and PbO [27]. In the meantime, when Sn contents are lower than 0.8 wt.%, Sn usually existed as Sn(II) and the passive layers are chiefly composed of mesoporous SnO[28] and Pb oxide[29]. Sn(II) can increase the pits per unit area of the PbO layers. Therefore the liquid among the gaps in PbO is the main ion transporter [30], which further enhanced the corrosion process. As the result of the enhancement of both ion and electron transportation, i_{corr} increases with Sn content of when it is below 0.8 wt.%.

When the Sn content is higher than 0.8 wt.%, alloying Sn would primarily segregate as Sn(IV) along the grain boundaries, and a little amount of Sn(II) dissolves inside the PbO matrix[12]. SnO_2 was very stable, making it difficult to form lower valency oxides. Therefore, the transportation rate of Sn ions along with grain boundaries could be reduced by SnO_2. As a result, although the conductivity, i.e., electron transportation, of the alloy could be further increased, ion transportation becomes the controlling step of the corrosion process, slowing down by increasing Sn contents in the alloy. The corrosion rate decreases when the weight percent of Sn increases from 0.8 to 1.5 wt.%, ultimately reaching a plateau at 1.5 wt.% Sn.

When the Sn content is above 2.6 wt.%, it has been found that there is excessive Sn segregated at the grain boundaries, which led to severe intergranular corrosion. The intergranular corrosion destroyed the integrity of the passive layer [19], causing the corrosion rate to bounce up. It should be mentioned that oxygen overvoltage data in Ref. [8] shows that Pb-Sn alloy has the best corrosion resistance when Sn con-

tent is between 2.0 and 3.0 wt.%, which is in accordance with the conclusion made in this investigation.

In general, Sn affects the corrosion of Pb-Sn alloys in H_2SO_4 solution by changing the kinetics of ion and electron transportation. When the Sn content is below 0.8 wt.%, the corrosion process is accelerated by the enhancement of both ion and electron transportation with increasing Sn contents. When Sn contents are between 0.8 and 1.5 wt.%, ion transportation is the controlling step of the corrosion process and it is decelerated by increasing Sn contents. When the Sn content is above 2.6 wt.%, corrosion rate is increased by excessive Sn segregation and intergranular corrosion.

4.4. Kinetics of cathodic reaction

It is well accepted that cathodic reaction of Pb-Sn corrosion is a single-step process, so n_C should be close to unity. However, It is indicated in Table 5 that during the oxidation process of Pb-Sn alloys in H_2SO_4, the calculated n_C for specimens Nos. 1, 2, 3 and 5 is around 0.5, which does not match the "*single-electron transfer*" theory. Therefore, one can be proposed that there might be "*half-electron transfer*" phenomenon during the electrochemical process.

During the reactions of Nos. 1, 2, 3 and 5 alloys, when two hydrogen cations reached the surface of the electrode, they could obtain one electron to form H_2^+, and then H_2^+ kept attaining electrons to form hydrogen molecules. The two-step process can be expressed as:

$$\text{Sub-step 1}: \quad 2H^+ + e = {H_2}^+$$

$$\text{Sub-step 2}: \quad {H_2}^+ + e = H_2$$

Sub-step 1 could be the controlling step of the cathodic reaction. Therefore, the reaction rate can be calculated by:

$$i = i_0 \left[\exp\left(\frac{\alpha n F \eta}{RT} \right) - \exp\left(-\frac{\beta n F \eta}{RT} \right) \right] \tag{6}$$

In the Tafel zone, the negative exponential term, i.e. the second term on the right side of Eq. (6), could be neglected, and then taking the logarithm to both sides of the equation, we get:

$$\eta = -\frac{2.3RT}{\alpha n F} \log i_0 + \frac{2.3RT}{\beta n F} \log i \quad \text{or}$$

$$\eta = -\frac{2.3RT}{\beta n F} \log i_0 + \frac{2.3RT}{\beta n F} \log i \tag{7}$$

Assuming that both of the transport coefficients (α, β) are 0.5 ($\alpha + \beta = 1$), at the temperature of 290 K, the Tafel slope, b is 0.23 V. Considering the error of the transport coefficient, this result is in accordance with the experimental data. Since sub-step 1 can be expressed as $H^+ + 1/2e = 1/2{H_2}^+$, the phenomena can be named as "*half-electron transfer*".

Regarding the cathodic reaction of sample No. 6 (Pb-2.6 wt.% Sn), "*quarter-electron transfer*" ($1/4e^-$) is inferred to exist. The electrochemical process is assumed as follows:

$$\text{Sub-step 1}: \quad 4H^+ + e = {H_4}^{3+}$$

$$\text{Sub-step 2}: \quad {H_4}^{3+} + e = 2{H_2}^+$$

$$\text{Sub-step 3}: \quad {H_2}^+ + e = H_2$$

Among all the sub-steps $4H^+ + e = {H_4}^{3+}$ could be the controlling one. Following this assumption, the Tafel slope (b) of No. 6 is obtained as 0.46 V, which has good agreement with the experimental result.

For the sample No. 4 (Pb-1.57 wt.% Sn), the assumption of single-step anodic reaction gives Tafel slope b as 0.12 V, which is close to the experimental result.

The above analysis and calculations show that the cathodic reaction does not have to be a single-step process, i.e., there are multiple sub-steps involved and complex cations, including ${H_4}^{3+}$ and ${H_2}^+$, exist in the systems. The kinetic process of the cathodic reaction is different for the Pb-Sn alloys with various Sn contents.

5. Conclusions

In this paper, the effect of Sn concentration on the corrosion resistance of Pb-Sn alloy in H_2SO_4 was investigated by potentiodynamic polarization. A new approach was proposed to calculate i_{corr} by using a tested cathodic Tafel line and a weak polarization area. Other electrochemical parameters, such as n, a_A, and b_A, can also be calculated as by-products of this method. This new approach proved to be in accordance with the experimental results. Several conclusions can be drawn from this investigation:

1. Pb-Sn alloys have good anticorrosive properties in sulfur acid. During the potentiodynamic polarization process, pitting takes place above the potential E_p around 1.65 V when the passive films formed on the surface of alloys are penetrated.
2. Sn affects the corrosion of Pb-Sn alloys in H_2SO_4 solution by changing the kinetics of ion and electron transportation. When the Sn content is below 0.8 wt.%, the corrosion process is accelerated by the enhancement of both ion and electron transportation with increasing Sn contents. When Sn contents are between 0.8 and 1.5 wt.%, ion transportation is the controlling step of the corrosion process and it is decelerated by increasing Sn contents. When the Sn content is above 2.6 wt.%, the corrosion rate is increased because of excessive Sn segregation and intergranular corrosion.
3. The cathodic reaction does not have to be a single-step process, i.e., there are multiple sub-steps involved and complex cations, including ${H_4}^{3+}$ and ${H_2}^+$, existing in the systems. The kinetic process of the cathodic reaction is different for the Pb-Sn alloys with various Sn contents.

References

[1] X. Pindi, H. Liu, Basic Theory and Processing Mechanism of Lead Acid Battery, first ed., Shanghai Industrial Press, Shanghai, 1993, pp. 41–100.
[2] N.E. Bagsshaw, J. Power Sources 53 (1995) 25–30.
[3] E. Cattaneo, H. Stumpf, H.G. Tillmann, J. Power Sources 67 (1997) 283–289.
[4] Yasuha et al., U.S. Patent, 4,805,277.
[5] H. Giess, C. Ohlin, INTELEC proceedings, IEEE, 1996, pp. 334–343.
[6] A. Siegmund, E.D. Prengaman, JOM 53 (2001) 38–39.
[7] G. Hong, W. Zhang, Power Supply Techniq. 4 (1993) 1–5.
[8] H. Larsen, U.S. Patent 6,423,451.
[9] C.S. Lakshmi, J.E. Manders, D.M. Rice, J. Power Sources 73 (1998) 23–29.
[10] L. Bouirden, J.P. Hilger, J. Hertz, J. Power Sources 33 (1991) 27–50.
[11] H. Yasuda et al., U.S. Patent 4,939,051.
[12] L. Alber, A. Chabro, L. Torcheux, J. Power Sources 67 (1997) 257–265.
[13] E.M.L. Valeriote, A. Heim, M.S. Ho, J. Power Sources 33 (1991) 187–212.
[14] B. Monahov, D. Pavlov, A. Kirchev, S. Vasilev, J. Power Sources 113 (2003) 281–292.
[15] D. Pavlov, K. Kirchet, M. Stoycheva, B. Monahov, J. Power Sources 137 (2004) 288–308.
[16] B. Monahov, D. Pavlov, J. Electrochem Soc. 141 (1994) 2316–2326.
[17] Smithell's Metal Reference Book, eighth ed., Elsevier & ASM Intl., 2004.
[18] D. Yang, Z. Shen, Metallurgical Corrosion, second ed., Metallurgical Press, Beijing, 1999, pp. 19–41.
[19] R.F. Nelson, D.M. Wisdom, J. Power Sources 33 (1991) 165–185.
[20] J. Rowlette, S. Alkaitis, N. Pinsky, J.Y. Josefowicz, Energy Conversion Engineering Conference, San Diego, CA 1052, August 1986, 1986, pp. 25–29.
[21] M.N.C. Ijomah, J. Electrochem. Soc. 134 (1987) 2960–2965.
[22] M.N.C. Ijomah, J. Appl. Electrochem. 18 (1988) 142.
[23] G. Amran, Steyer, J. Steinmetz, J. Power Sources 64 (1997) 35–37.
[24] P. Simon, N. Bui, F. Dabosi, G. Chatainier, M. Provincial, J. Power Sources 52 (1994) 31–39.
[25] D. Hardy, R. Marx, J. Power Sources 38 (1992) 75–85.
[26] R. Ciu, S. Wang, J. Power Sources 46 (1993) 327–333.
[27] H. Giess, D. Pavlov, Proc. Electrochem. Soc. 84 (1984) 241.
[28] K. Salmi, G. Sundholm, J. Power Sources 40 (1992) 217–224.
[29] J. Xu, X. Li, X. Liu, C. Dong, N. Deem, Met. Mat. Trans. A, 2005, in press.
[30] H. Liu, C. Yang, J. Power Sources 103 (2002) 173–179.